nature nanotechnology

LETTERS

https://doi.org/10.1038/s41565-020-00794-z

Check for updates

Long-lived modulation of plasmonic absorption by ballistic thermal injection

John A. Tomko[1], Evan L. Runnerstrom[2,3], Yi-Siang Wang[4,5], Weibin Chu[4,5], Joshua R. Nolen[6], David H. Olson[7], Kyle P. Kelley[3], Angela Cleri[8], Josh Nordlander[8], Joshua D. Caldwell[6], Oleg V. Prezhdo[4,5], Jon-Paul Maria[3,8] and Patrick E. Hopkins[1,7,9]✉

Light–matter interactions that induce charge and energy transfer across interfaces form the foundation for photocatalysis[1,2], energy harvesting[3] and photodetection[4], among other technologies. One of the most common mechanisms associated with these processes relies on carrier injection. However, the exact role of the energy transport associated with this hot-electron injection remains unclear. Plasmon-assisted photocatalytic efficiencies can improve when intermediate insulation layers are used to inhibit the charge transfer[5,6] or when off-resonance excitations are employed[7], which suggests that additional energy transport and thermal effects could play an explicit role even if the charge transfer is inhibited[8]. This provides an additional interfacial mechanism for the catalytic and plasmonic enhancement at interfaces that moves beyond the traditionally assumed physical charge injection[9–12]. In this work, we report on a series of ultrafast plasmonic measurements that provide a direct measure of electronic distributions, both spatially and temporally, after the optical excitation of a metal/semiconductor heterostructure. We explicitly demonstrate that in cases of strong non-equilibrium, a novel energy transduction mechanism arises at the metal/semiconductor interface. We find that hot electrons in the metal contact transfer their energy to pre-existing free electrons in the semiconductor, without an equivalent spatiotemporal transfer of charge. Further, we demonstrate that this ballistic thermal injection mechanism can be utilized as a unique means to modulate plasmonic interactions. These experimental results are well-supported by both rigorous multilayer optical modelling and first-principle ab initio calculations.

We hypothesize a novel interfacial energy transduction mechanism that arises from the non-equilibrium dynamics at metal/semiconductor interfaces when electron temperatures are highly elevated relative to the crystal lattice temperature at ultrafast timescales. In this regime, interfacial energy injection (without a similar concomitant charge injection) from an excited metal to a non-metal offers the possibility to remotely manipulate the photonic and electronic properties of non-metals without relying on specific photonic or electronic excitations in the non-metal or metal contact. This would enable remote control of the non-metal's functional properties via solely energy transfer and lead to the potential for new classes of material heterostructures and technologies in which the optical and electrical functional performances are controlled by heat.

To test this hypothesis, we must identify a system that lacks facile charge injection across a metal/semiconductor interface when in an excited state. Electron injection and/or interfacial electronic thermal diffusion occurs in response to a gradient in the electronic chemical potential or Fermi level induced by an extrinsic perturbation (for example, photonic excitation, temperature differences or applied bias). Additionally, for charge to traverse across a boundary, the excited carriers must have enough energy to overcome or tunnel through any Schottky barrier that exists at the interface. However, what happens when the excited carriers are not accompanied by a change in the electronic chemical potential? How do charge and heat in a spatially homogeneous chemical potential flow across an ohmic contact? We address these questions by studying the ultrafast thermal transport mechanisms across gold/yttrium-doped cadmium oxide (Au/Y:CdO) interfaces with a variety of subpicosecond pump–probe measurements. When described by a near-equilibrium Fermi–Dirac distribution, the electrons in Au have a nearly temperature-independent electronic chemical potential[13]; as such, when excited by an absorbed energy pulse, there is no driving force for the transfer of charge, but there is an energy gradient that drives the transfer of heat. Further, Au forms a barrier-free ohmic contact with Y:CdO, a degenerate semiconductor. In concert, these two effects should eliminate the ability for light-induced charge transfer to occur at this metal/semiconductor interface at picosecond and longer timescales.

With these two factors in mind, charge carriers are not expected to flow between two materials after a pulsed excitation of conduction electrons in Au. Importantly, the weak electron–phonon coupling factor of Au allows its excited electrons to stay at highly elevated temperatures for prolonged times relative to those of other metals. Thus, after the ultrafast excitation of Au, energy can ballistically traverse the Au film through the electron subsystem to reach the Au/CdO interface, which can occur before the electron subsystem thermalizes with the phonons and loses its excess energy to the Au lattice subsystem. As this energy front in Au reaches the Au/CdO interface, the hot-electron subsystem in Au can then directly couple excess energy into CdO's electron subsystem due to the strong overlap of electronic wavefunctions between the two materials. This results in a ballistic energy transduction across the

[1]Department of Materials Science and Engineering, University of Virginia, Charlottesville, VA, USA. [2]Army Research Office, CCDC US Army Research Laboratory, Research Triangle Park, NC, USA. [3]Department of Materials Science and Engineering, North Carolina State University, Raleigh, NC, USA. [4]Department of Chemistry, University of Southern California, Los Angeles, CA, USA. [5]Department of Physics and Astronomy, University of Southern California, Los Angeles, CA, USA. [6]Institute of Nanoscale Science and Engineering, Vanderbilt University, Nashville, TN, USA. [7]Department of Mechanical and Aerospace Engineering, University of Virginia, Charlottesville, VA, USA. [8]Department of Materials Science and Engineering, Pennsylvania State University, State College, PA, USA. [9]Department of Physics, University of Virginia, Charlottesville, VA, USA. ✉e-mail: phopkins@virginia.edu

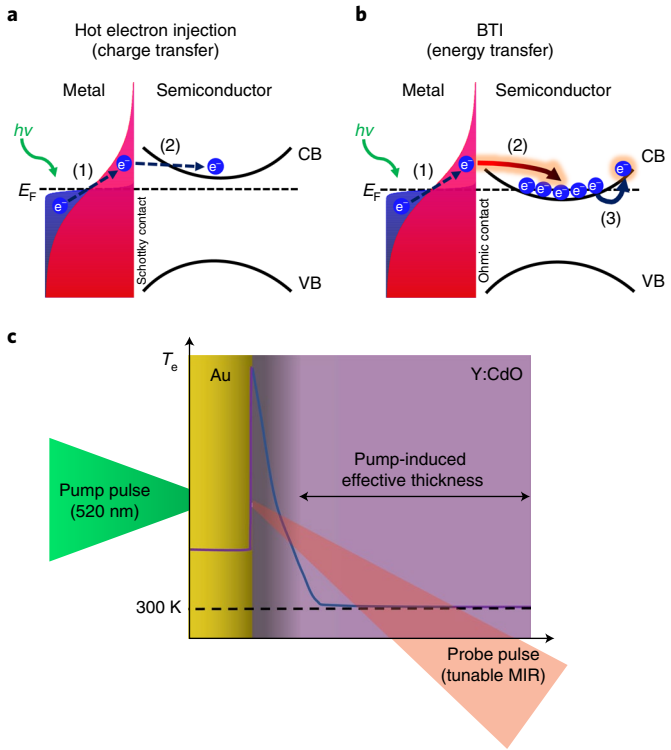

Fig. 1 | Proposed mechanism of interfacial energy transfer and experimental schematic. a, Hot electron injection: the process typically assumed to occur at metal/semiconductor interfaces after photoexcitation of the metallic contact. In this case, hot electrons are first generated in the Au (1). At sufficiently high electron temperatures, the electrons traverse the interface and add charge to the conduction band (CB) of the semiconductor (2). **b**, Ballistic thermal injection (BTI): our proposed process for metal/semiconductor interfaces after an ultrafast excitation of the metal contact. This mechanism relies on hot-electron generation in the metal (1); prior to the electron–phonon coupling (less than a couple of picoseconds), energy propagates ballistically towards the metal/semiconductor interface. The electron energy front reaches the interface, whereby the electrons transfer their energy (2), rather than charge, to the pre-existing free electrons in the semiconductor's conduction band. The pre-existing semiconductor's electrons are now at an elevated temperature (see electron temperature profile in **c**, depicted by the purple and blue curves), and are promoted to elevated states in the conduction band (3) (for example, intraband excitations). Note that the scattering processes after either charge injection or the proposed BTI energy transfer mechanism, such as hot electron–electron scattering, are excluded for clarity. **c**, Schematic of our ultrafast ENZ experiment to spatially resolve the electron energy distribution after the potential injection processes. The 520 nm pump beam excites the Au surface at the Au/air interface, and a subpicosecond probe pulse monitors the ENZ mode of a thin Y:CdO film. E_F, Fermi energy; MIR, mid-infrared; T_e, electron temperature; VB, valence band.

interface with a relatively negligible charge transfer, which we refer to as ballistic thermal injection (BTI). Schematics of the typically assumed charge-injection process and our proposed BTI process are shown in Fig. 1a,b, respectively.

In addition to the unique ability to separate energy and charge transfer processes, doped CdO is a model mid-infrared plasmonic material that supports free electron densities on the order of 10^{19}–10^{21} cm^{-3} while maintaining high electron mobilities of 300–500 cm^{-2} V^{-1} s^{-1} (refs. [14–16]). These electronic properties enable strong, sharp and resonant light–matter interactions at mid- to near-infrared frequencies. As in other plasmonic materials, these resonances are highly sensitive to local changes in the electronic environment, which include electron density, effective mass and dielectric constant. A key difference here is that, rather than probing the surface and environment-sensitive surface plasmon polaritons, as is common in thin-film metallic plasmonics, we optically monitored the resonant radiative bulk epsilon-near-zero (ENZ) mode (also known as the Brewster mode) of the CdO after the optical excitation of the Au film. Our sample geometry was especially convenient for this experiment, as the Au film also acted as a mirror that enhanced the free-space coupling of the ENZ mode, which allowed us to monitor the reflectivity of the CdO/Au heterostructure from the backside through a transparent substrate. Owing to the high electronic mobility of our Y:CdO, the ENZ mode manifested as a sharp resonant dip in the reflectivity (that is, an absorption peak), which made it straightforward to resolve changes in the optical behaviour. This scheme provides high sensitivity to the spatial distribution of electronic energy in the semiconductor as well as its temporal evolution after energy transfer from the metallic film; a schematic of this measurement technique and the sample configuration is shown in Fig. 1c, and greater detail can be found in the Supplementary Information. In the following, we demonstrate the long-lived modulation of the CdO ENZ mode after Au excitation, and show that this modulation can be explained by the BTI process and not by a charge transfer mechanism.

To gain initial insight into the hot-electron dynamics at the Au/CdO interface, and ensure our hypothesis of BTI can occur in these systems, we first performed time-domain thermoreflectance (TDTR) measurements[17,18] on the Au/CdO samples supported by sapphire (Al_2O_3) substrates, in which both the pump and probe were focused on the top Au film/air interface. These measurements allowed us to quantify the ultrafast energy flow across the Au/CdO and CdO/substrate interfaces and assess the timescales of thermal transport at each interface. A description to provide a conceptual understanding of the ultrafast TDTR data is provided in the Supplementary Information and Supplementary Fig. 1.

Our TDTR measurements (Fig. 2a) on the 15 nm Au/100 nm CdO films display the signature 'back-heating' from subsurface energy deposition and transient thermal diode effects from the more-efficient ballistic injection of energy across an interface than that of diffusive flow of heat towards the surface. This indicates that hot electrons in the Au transferred their energy to free electrons in the CdO at ultrafast timescales[17,19]. Conversely, when a thin 15 nm dielectric HfO_2 layer was placed between the Au and CdO, this energy transfer process was inhibited and no signs of back-heating or transient diode effects were observed. This observation also rules out any possibility that the pump beam directly excites the CdO film and is the cause for subsurface heating or optically spurious signals, as the HfO_2 is optically transparent to the pump wavelength. It also confirms our posit that this 15-nm dielectric barrier, which limits the electron wavefunction overlap between Au and CdO, will inhibit thermal energy transduction across the Au/CdO interface.

As mentioned, interpreting the spectroscopic characteristics in typical pump–probe experiments, such as TDTR, can be quite difficult, as several mechanisms can lead to nearly identical signatures. In both metal/metal and Au/CdO heterostructures, there are two potential mechanisms for subsurface heating at ultrafast timescales: charge injection and our proposed BTI process. In both situations, an ohmic contact between the two materials with a high carrier density may lead one to expect facile charge injection into the underlying metal or, in our case, the degenerately doped semiconductor CdO. In this case, the injected electron would eventually decay within the CdO via electron–phonon coupling and induce a subsurface temperature rise. Contrarily, the back-heating signatures could result from BTI without any concomitant charge flow: optically deposited energy ballistically traverses Au's electronic subsystem to reach the interface, where it efficiently couples energy directly to the

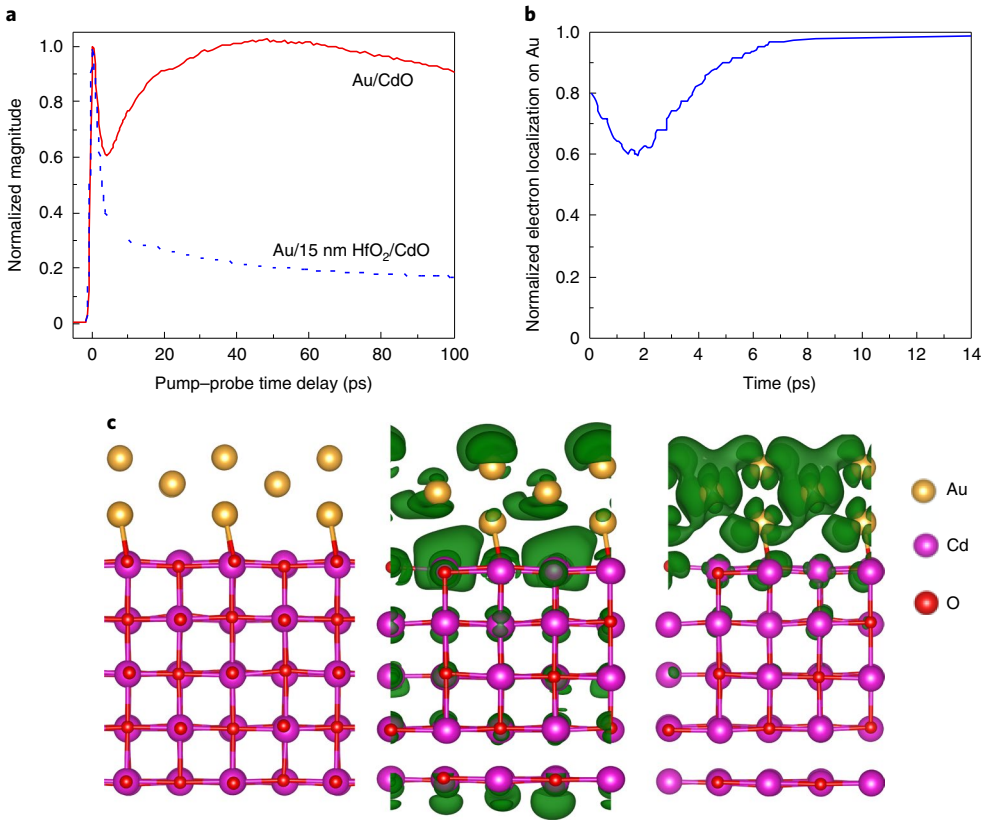

Fig. 2 | Interpreting subsurface heat deposition with ab initio calculations. a, TDTR curves for 15 nm Au on 100 nm CdO with a carrier concentration of 7.7×10^{19} cm^{-3}. In the case that the two are in direct contact (red line), back-heating is clearly observed, indicative of electron injection. Conversely, the addition of a thin dielectric layer between the two media (dashed blue line) inhibits this injection effect and leads to electron thermalization only within the Au film. **b**, Evolution of electron localization on Au atoms; zero time corresponds to the initially excited state. Although the electron remains primarily localized within the Au slab, its wavefunction extends into the CdO, which allows for a greatly increased energy transfer rate due to the high-frequency modes available within the CdO. After a few picoseconds, as the structure relaxes, the electron relocalizes solely within the Au layer, which thus ends the BTI process. **c**, Left: optimized structure of the Au/CdO simulation cell. The CdO slab is about twice as thick as the Au slab, which mimics the experiments. Middle and right: charge densities of the initial ($t = 0$ ps) pumped (middle) and final ($t = 14$ ps) (right) states, respectively. The excited hot electron localized on Au has a tail into CdO. The relaxed electron is localized nearly fully on Au, because the Au Fermi level is inside the CdO bandgap.

electronic subsystem of the underlying CdO. After this BTI process, the now-excited electrons in the underlying CdO would couple to the lattice and lead to subsurface heating.

To distinguish the charge injection versus BTI processes, we simulated the electronic interactions involved in the non-equilibrium photoinduced dynamics via ab initio real-time time-dependent density functional theory (TDDFT) for electrons coupled to non-adiabatic molecular dynamics (NAMD) for atomic motions (Fig. 2c). The calculations reveal that, after photoexcitation of the Au, the hot electron remains within the Au and the tail of its wavefunction extends into the CdO layer. This tail directly couples energy to electrons in the CdO within picoseconds, followed by electron–phonon relaxation through high-frequency phonon modes[20]. Concurrently, the hot electron's wavefunction quickly (~6 ps) relocalizes within the Au (Fig. 2b,c), which quenches the BTI. The calculations show that energy transfer from Au to CdO is mediated by hot-electron-energy coupling and not a phononic or charge-injection process. This result, obtained with small representations of the Au/CdO interface, agrees well with our observed experimental trends and supports the two-temperature interpretation of our results.

This BTI mechanism offers a unique opportunity to manipulate the electrons in an optically active material through injected heat as opposed to relying on direct photonic or electronic perturbations, as is commonly done. Instead, the BTI process remotely manipulates the photonic or electronic response of a non-metal through optical excitation of the metal transducer. To demonstrate this, we performed additional pump–probe experiments on the heterostructure, in which a tunable infrared probe monitored the ENZ behaviour of the CdO after visible (520 nm) excitation of the Au film at picosecond timescales. This ENZ mode is highly sensitive to the electronic environment and free carrier dynamics within the CdO. By monitoring CdO's optical behaviour, we gained direct knowledge of how the electronic environment changed with time during the BTI process. See the Supplementary Information for additional details on the ENZ modes and this experiment.

With the pump excitation of Au, the ENZ absorption peak of CdO at ~3,800 nm redshifted, which increased the absorption (decreased the reflectivity) at longer wavelengths. Concurrently, the absorption (reflectivity) decreased (increased) at shorter wavelengths, though to a lesser extent. This asymmetric redshift persisted for hundreds of picoseconds after the thermal excitation of the Au film.

Our observation of a redshift immediately negates the possibility of electron injection from the Au into the CdO layer. Based on the Drude model, the ENZ mode of a conducting thin film is centred at the screened plasma frequency, $\omega_{ENZ} = \omega_p/\sqrt{\epsilon_\infty}$, where ϵ_∞ is the high-frequency dielectric constant, $\omega_p = \sqrt{n_e e^2/m^* \epsilon_0}$, and where n_e is the free electron density and m^* is the effective mass of the

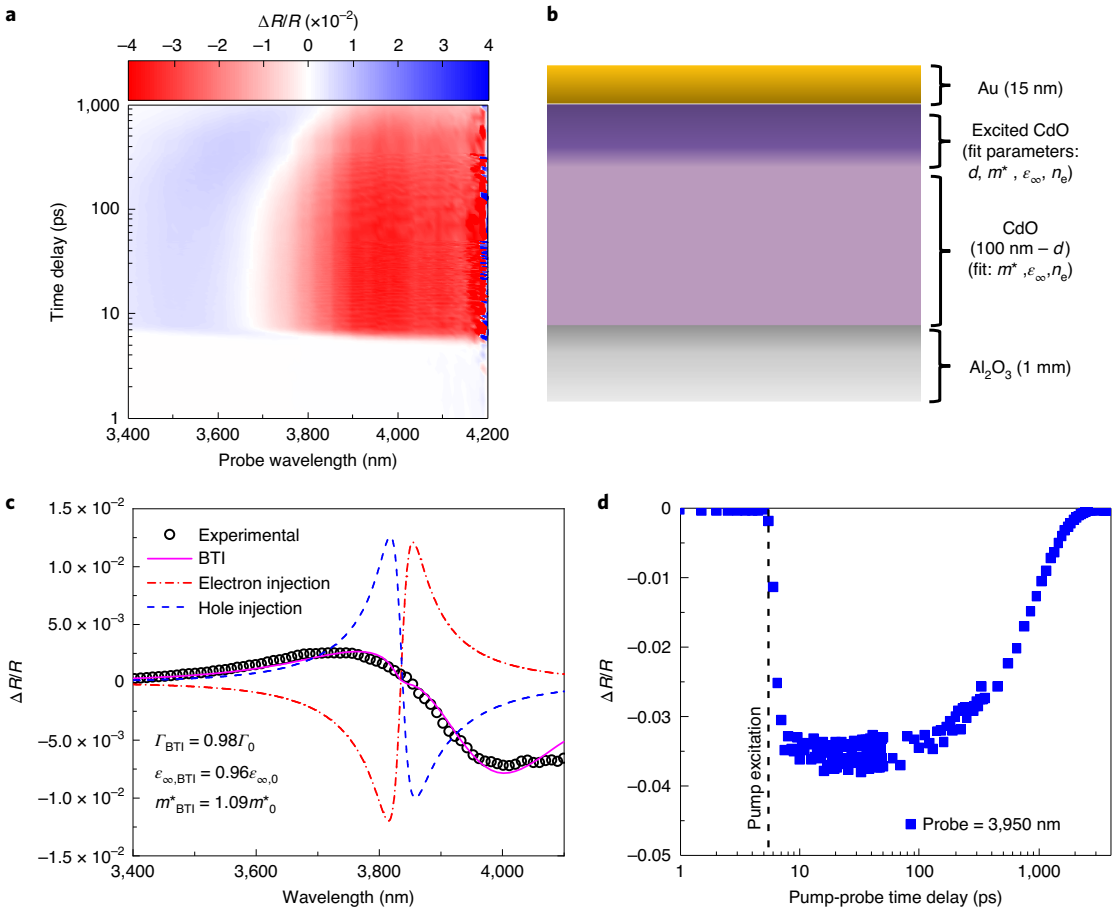

Fig. 3 | Ultrafast plasmonic modulation through BTI. a, Transient reflectivity (R) measurements at a fluence of ~0.5 J m^{-2}. The x axis denotes the wavelength of the probe beam, and the y axis represents the time delay between the 520 nm pump pulse and the tunable infrared probe beam; the spectral resolution of these data is 10 nm. Note, the pump pulse arrives at ~6 ps. Additionally, red represents a decrease in probe reflectance, whereas blue represents an increased reflectance. **b**, Schematic of the TMM simulation along with the various fit parameters. **c**, Change in R for the Au/CdO heterostructure immediately after pump excitation and the simulated reflectance curves calculated via the TMM for various injection mechanisms. Clearly, neither hole nor electron injection are able to capture the observed trend. The inset values are the TMM best-fit values, which determined a 5 nm perturbation layer (the layer thickness, d, is a fitting parameter), in agreement with our two-temperature model calculations. The best-fit values represent the change in Drude model parameters (electron scattering rate, Γ, high-frequency permittivity, ϵ_∞, and effective mass, m^*, for the 5 nm heated CdO layer after ultrafast heating of the Au film.) **d**, Transient R of the Au/CdO heterostructure probed at 3,950 nm after visible excitation of the Au film; the 1/e decay time of this curve is approximately 700 ps.

electrons. Therefore, any electron injection would increase n_e and result in a blueshift of the ENZ absorption peak, in direct contrast to our experimental results.

Although one could argue that hole injection or heating of the CdO layer may be occurring, which would result in a decrease in n_e and an increase in m^*, respectively, both would lead to a symmetric redshift. As indicated before and shown in Fig. 3a,c, we clearly observe an asymmetric redshift. To understand the origin of this asymmetry, we performed optical transfer matrix method (TMM, Fig. 3b,c) calculations to model how the electron distribution changes in the CdO layer after Au excitation (a more detailed description can be found in the Supplementary Information).

Our TMM calculations reveal that n_e remains unchanged in the CdO, regardless of pump fluence or the relative pump–probe time delay, which indicates that neither electron nor hole injection occurs. Rather, in accordance with our BTI hypothesis, the energy distribution of these charges changes based on the following physical processes. First, the Au couples its electronic energy to the CdO, and thus heats free electrons within a thin (<5 nm) CdO layer near the Au/CdO interface. This energy heats the electrons, which leads to a local increase in m^* within this layer[21]. Additionally, because the scattering rate is inversely proportional to the effective mass, our model also captures a local decrease in the damping frequency of the free electrons. As this heated layer is now out of equilibrium relative to the remainder of the CdO, electrons from the 'bulk' of the film diffuse towards the hot CdO layer, which temporarily forms an accumulation layer near the Au/CdO interface and slightly decreases n_e throughout the remainder of the CdO film. Note, this electron diffusion is permitted in CdO due to its temperature-dependent electron chemical potential, unlike the constant chemical potential associated with Au. This increase in the local number density leads to a corresponding decrease in the high-frequency permittivity, ϵ_∞ (refs. [22,23]). As shown in Fig. 3c, the TMM calculations only reproduce our experimental results, with excellent agreement, when our proposed BTI energy transfer mechanism is invoked. TMM-simulated electron or hole injection cannot explain the observed asymmetric redshift in ENZ absorption, regardless of whether the charge is injected into the full CdO layer or into a thin slab near the interface. We also note that a lack of 'net' charge

transfer, as observed in these ultrafast experiments, exists through pre-existing theories, namely via non-equilibrium electronic thermal diffusion (Supplementary Fig. 9). Although we cannot fully rule out the effects of this mechanism, we believe it may play a supporting role and operate in-tandem with the proposed BTI mechanism; additional details on this note can be found in the Supplementary Information.

Finally, we note that electronic non-equilibrium within the CdO, and thus the associated remote modulation of the ENZ mode, is altered for prolonged times with a $1/e$ decay time of approximately 700 ps (Fig. 3d). This length of modulation is orders of magnitude greater than those of previous works that investigated light-induced changes in the plasmonic absorption of the CdO film[21]. This long-lived modulation is ultimately enabled by the aforementioned transient thermal diode effect that is enabled by the BTI process across the Au/CdO interface.

In summary, we found that under non-equilibrium conditions, photoexcited metals can undergo an electron-mediated ballistic energy transfer process that can remotely modulate the electronic environment of an underlying degenerate semiconductor via heat. We termed this effect ballistic thermal injection (BTI) to distinguish it from the well-studied charge injection effects caused by hot electrons that traverse an energy barrier. From an application perspective, one could conceive of several applications in which longer optical or electronic modulation lifetimes are more beneficial than those that cannot be achieved via the more traditionally studied hot electron injection (carrier injection) across interfaces, such as catalysis, sensing or energy harvesting. The long-lived modulation of ENZ media, in particular, can be utilized as a selective emitter for thermophotovoltaic conversion, as BTI can prolong the desired state of emissivity, or non-linear phenomena, such as four-wave mixing and high harmonic generation. Furthermore, the proposed BTI energy transduction mechanism could provide an explanation for discrepancies between current theory and experimental results in light–matter interactions, such as photocatalysis, that rely on either the framework of a charge-transfer motif or solely phononic heat conduction.

Online content

Any methods, additional references, Nature Research reporting summaries, source data, extended data, supplementary information, acknowledgements, peer review information; details of author contributions and competing interests; and statements of data and code availability are available at https://doi.org/10.1038/s41565-020-00794-z.

Received: 24 January 2020; Accepted: 13 October 2020;
Published online: 9 November 2020

References

1. Serpone, N. & Emeline, A. V. Semiconductor photocatalysis—past, present, and future outlook. *J. Phys. Chem. Lett.* **3**, 673–677 (2012).
2. Kim, S. M., Hyosun, L. & Park, J. Y. Charge transport in metal-oxide interfaces: genesis and detection of hot electron flow and its role in heterogeneous catalysis. *Catal. Lett.* **145**, 299–308 (2015).
3. Clavero, C. Plasmon-induced hot-electron generation at nanoparticle/metal-oxide interfaces for photovoltaic and photocatalytic devices. *Nat. Photon.* **8**, 95–103 (2014).
4. Knight, M. W., Sobhani, H., Nordlander, P. & Halas, N. J. Photodetection with active optical antennas. *Science* **332**, 702–704 (2011).
5. Asapu, R. et al. Electron transfer and near-field mechanisms in plasmonic gold-nanoparticle-modified TiO_2 photocatalytic systems. *ACS Appl. Nano Mater.* **2**, 4067–4074 (2019).
6. Chen, J. J., Wu, J. C., Wu, P. C. & Tsai, D. P. Improved photocatalytic activity of shell-isolated plasmonic photocatalyst Au@SiO_2/TiO_2 by promoted LSPR. *J. Phys. Chem. C* **116**, 26535–26542 (2012).
7. Priebe, J. B. et al. Water reduction with visible light: synergy between optical transitions and electron transfer in Au–TiO_2 catalysts visualized by in situ EPR spectroscopy. *Angew. Chem. Int. Ed.* **52**, 11420–11424 (2013).
8. Yu, Y., Sundaresan, V. & Willets, K. A. Hot carriers versus thermal effects: resolving the enhancement mechanisms for plasmon-mediated photoelectrochemical reactions. *J. Phys. Chem. C* **122**, 5040–5048 (2018).
9. Narang, P., Sundararaman, R. & Atwater, H. A. Plasmonic hot carrier dynamics in solid-state and chemical systems for energy conversion. *Nanophotonics* **5**, 96–111 (2016).
10. Brongersma, M. L., Halas, N. J. & Nordlander, P. Plasmon-induced hot carrier science and technology. *Nat. Nanotechnol.* **10**, 25–34 (2015).
11. Sundararaman, R., Narang, P., Jermyn, A. S., Iii, W. A. G. & Atwater, H. A. Theoretical predictions for hot-carrier generation from surface plasmon decay. *Nat. Commun.* **5**, 5788 (2014).
12. Wu, K., Chen, J., McBride, J. R. & Lian, T. Efficient hot-electron transfer by a plasmon-induced interfacial charge-transfer transition. *Science* **349**, 632–635 (2015).
13. Lin, Z., Zhigilei, L. V. & Celli, V. Electron–phonon coupling and electron heat capacity of metals under conditions of strong electron–phonon nonequilibrium. *Phys. Rev. B* **77**, 075133 (2008).
14. Sachet, E. et al. Dysprosium-doped cadmium oxide as a gateway material for mid-infrared plasmonics. *Nat. Mater.* **14**, 414–420 (2015).
15. Runnerstrom, E. L., Kelley, K. P., Sachet, E., Shelton, C. T. & Maria, J. P. Epsilon-near-zero modes and surface plasmon resonance in fluorine-doped cadmium oxide thin films. *ACS Photon.* **4**, 1885–1892 (2017).
16. Runnerstrom, E. L. et al. Polaritonic hybrid-epsilon-near-zero modes: beating the plasmonic confinement vs propagation-length trade-off with doped cadmium oxide bilayers. *Nano Lett.* **19**, 948–957 (2019).
17. Choi, G.-M., Wilson, R. B. & Cahill, D. G. Indirect heating of Pt by short-pulse laser irradiation of Au in a nanoscale Pt/Au bilayer. *Phys. Rev. B* **89**, 064307 (2014).
18. Radue, E. L. et al. Hot electron thermoreflectance coefficient of gold during electron–phonon nonequilibrium. *ACS Photon.* **5**, 4880–4887 (2018).
19. Giri, A. et al. Mechanisms of nonequilibrium electron–phonon coupling and thermal conductance at interfaces. *J. Appl. Phys.* **117**, 105105 (2015).
20. Zhou, X. et al. Thin Ti adhesion layer breaks bottleneck to hot hole relaxation in Au films. *J. Chem. Phys.* **150**, 184701 (2019).
21. Yang, Y. et al. Femtosecond optical polarization switching using a cadmium oxide-based perfect absorber. *Nat. Photon.* **11**, 390–395 (2017).
22. Liu, C. P. et al. Effects of free carriers on the optical properties of doped CdO for full-spectrum photovoltaics. *Phys. Rev. Appl.* **6**, 064018 (2016).
23. Nolen, J. R. et al. Ultraviolet to far-infrared dielectric function of *n*-doped cadmium oxide thin films. *Phys. Rev. Mater.* **4**, 02520 (2020).

Methods

Sample fabrication. Heteroepitaxial thin films of Y-doped CdO were prepared by reactive high-power impulse magnetron sputtering from a metallic Cd target and by reactive radio-frequency sputtering from a metallic Y target. All the films were grown on epitaxial-polished Al_2O_3. Film thicknesses were determined by X-ray reflectivity measurements. Finally, 15 nm of Au was deposited via electron-beam evaporation.

TDTR. To gain insight into the temperature response of the Au film after pulsed excitation, we performed and repeated TDTR measurements on two different systems; these are identical in all aspects, except that one is two-tint (for example, the pump and probe are both centred at a wavelength of 800 nm) and the other is two colour (for example, the pump is frequency doubled via a bismuth tri-borate crystal to a wavelength of 400 nm and the probe operates at the fundamental 800 nm output). In both cases, the pump beam was modulated at 8.8 MHz and focused to the sample surface.

Optical pump–infrared probe measurements. To monitor the ENZ condition of the doped CdO film after excitation of the Au film, we utilized a second pump–probe system to measure the differential reflectivity. This experiment relies on a 400 fs laser operating at its fundamental wavelength of 1,040 nm with a repetition rate of 500 kHz (Spectra Physics 30W Spirit-HP). The output was split into two paths. The first path is frequency doubled to a wavelength of 520 nm, which operates as the pump pulse. This pump was passed down a mechanical delay stage, mechanically chopped at a frequency of 451 Hz, and then focused to the surface of the Au metal film at the Au/air interface. The other portion of the beam was passed through an optical parametric amplifier, in which the signal beam was filtered out and the idler operated as the probe; this probe beam was spectrally varied in 10 nm increments from 3,400 to 4,200 nm and focused onto the Au surface at the CdO/Au interface. The sapphire/100 nm CdO/Au sample was mounted on a mechanical goniometer to allow for a high precision in defining the incident angle of the probe beam. Although the ENZ resonance for this structure had a minimal angular dependence and inhibited reflection at the plasma frequency from 30 to 70°, the peak absorption occurred at 55°, at which we thus performed the majority of our experiments. Note, the probe beam was *p*-polarized for the majority of our experimental results as only this polarization is sensitive to the ENZ mode.

TDDFT. The non-equilibrium dynamics of coupled electrons and nuclei were simulated by real-time TDDFT for the electronic evolution coupled to ionic motions via NAMD. The simulation cell was formed from five layers of CdO and three layers of Au atoms to imitate the experimental thickness ratio of the CdO and Au films, and 20 Å of vacuum separated the slabs. The simulation cell contained 138 atoms in total, which included 60 Cd, 60 O and 18 Au atoms. The geometric and electronic structure calculations and adiabatic molecular dynamics are carried out with Quantum Espresso[24,25]. The simulations use the PBE functional, an 820 eV energy cutoff for the plane-wave basis set and a $4\times6\times1$ *k*-point mesh grid. After the structure optimization, the system was brought up to 300 K in the canonical ensemble using the Andersen thermostat. Then, a 5 ps trajectory was obtained in the microcanonical ensemble and used for the subsequent NAMD simulations. The adiabatic state energies and nonadiabatic (NA) coupling were calculated for each step of the molecular dynamics run. The 5 ps NA Hamiltonian obtained in this way was iterated several times to simulate longer time dynamics. The nuclear dynamics of the system was rather simple, as it involved no long-term atomic rearrangements, and therefore 5 ps were sufficient to sample the nuclear motions that drive the electron dynamics (see Supplementary Fig. 3 for the electron–phonon relaxation). The NAMD calculations were carried out using the quantum-classical fewest-switches surface hopping technique implemented with real-time TDDFT in the PYXAID code[26,27]. The initial 1,000 geometries were sampled from the 5 ps molecular dynamics trajectory, and 100 stochastic realizations of the fewest-switches surface hopping process were generated for each geometry. Additional details on the TDDFT/NAMD calculations can be found in the Supplementary Information, which includes the relative electron density of states of the Au/CdO system (Supplementary Fig. 2) and the phonon frequencies of the system (Supplementary Fig. 4).

Additional calculations performed with thicker Au and CdO slabs (Supplementary Figs. 5–8) demonstrate a similar shift of wavefunction localization from Au to CdO, and then back to Au. The localization shift required a longer time in thicker slabs, and slowly approached the experimental result (Fig. 2a). The electron–phonon relaxation became slightly slower in the thicker slabs at the earlier times, because Au atoms are heavier than CdO atoms.

Data availability

The data that support the plots within this paper and other findings of this study are available from the corresponding author upon reasonable request.

References

24. Giannozzi, P. et al. Quantum Espresso: a modular and open-source software project for quantum simulations of materials. *J. Phys. Condens. Matter* **21**, 395502 (2009).
25. Giannozzi, P. et al. Advanced capabilities for materials modelling with Quantum Espresso. *J. Phys. Condens. Matter* **29**, 465901 (2017).
26. Akimov, A. V. & Prezhdo, O. V. The PYXAID program for non-adiabatic molecular dynamics in condensed matter systems. *J. Chem. Theory Comput.* **9**, 4959–4972 (2013).
27. Akimov, A. V. & Prezhdo, O. V. Advanced capabilities of the PYXAID program: integration schemes, decoherence effects, multiexcitonic states, and field-matter interaction. *J. Chem. Theory Comput.* **10**, 789–804 (2014).

Acknowledgements

We acknowledge funding from the US Department of Defense, Multidisciplinary University Research Initiative through the Army Research Office, Grant no. W911NF-16-1-0406. J.R.N. and J.D.C. appreciate support from the Office of Naval Research, Grant no. N00014-18-1-2107.

Author contributions

P.E.H. and J.-P.M. conceived the idea and supervised the project; J.A.T. performed the TDTR and infrared pump–probe measurements and corresponding analysis; E.L.R., K.P.K., J.N. and A.C. grew and characterized the CdO films; Y.-S.W., W.C. and O.V.P. performed the ab initio calculations; J.A.T. and D.H.O. performed the two-temperature model (TTM) calculations; J.A.T., J.R.N. and J.D.C. performed the transfer matrix method (TMM) calculations and provided insight on the dispersion relations. J.A.T. wrote the manuscript with input from all the authors; all the authors discussed the results and commented on the manuscript.

Competing interests

The authors declare no competing interests.

Additional information

Supplementary information is available for this paper at https://doi.org/10.1038/s41565-020-00794-z.

Correspondence and requests for materials should be addressed to P.E.H.

Peer review information *Nature Nanotechnology* thanks the anonymous reviewers for their contribution to the peer review of this work.

Reprints and permissions information is available at www.nature.com/reprints.